# Thermoluminescence investigation of donor ($Ce^{3+}$, $Pr^{3+}$, $Tb^{3+}$) acceptor ($Eu^{3+}$, $Yb^{3+}$) pairs in $Y_3Al_5O_{12}$

Fangtian You,[1,2,*] Adrie J. J. Bos,[1] Qiufeng Shi,[2] Shihua Huang,[2] and Pieter Dorenbos[1]

[1]*Faculty of Applied Sciences, Delft University of Technology, Mekelweg 15, 2629 JB Delft, The Netherlands*

[2]*Key Laboratory of Luminescence and Optical Information, Ministry of Education, Institute of Optoelectronic Technology, Beijing Jiaotong University, Beijing 100044, P.R. China*

(Received 8 November 2011; revised manuscript received 12 January 2012; published 1 March 2012)

The thermoluminescence properties of $Y_3Al_5O_{12}$ (YAG) doped with an electron donor lanthanide ($Ce^{3+}$, $Pr^{3+}$, or $Tb^{3+}$) together with an electron acceptor lanthanide ($Yb^{3+}$ or $Eu^{3+}$) were studied with the aim to locate the energy levels of each divalent and each trivalent lanthanide within the band gap. The activation energies needed to liberate electrons trapped by $Yb^{3+}$ or $Eu^{3+}$ were determined from thermoluminescence heating rate plots. With an automated thermoluminescence excitation spectroscopy technique, information on the energy level location of the electron donors $Ce^{3+}$, $Pr^{3+}$, and $Tb^{3+}$ was obtained. By combining all data with an empirical model, a scheme containing all the divalent and trivalent lanthanide energy levels in YAG has been constructed.

DOI: 10.1103/PhysRevB.85.115101 PACS number(s): 78.55.−m, 78.47.−p, 78.60.−b

## I. INTRODUCTION

Lanthanide-activated compounds provide the most important contribution to phosphors for lighting and display applications due to the numerous optical transitions possible between the $4f$ or $5d$ levels of the lanthanides. The application of lanthanide-doped phosphors can be hindered by a too-poor quantum efficiency of luminescence, which depends strongly on the absolute position of the lanthanide energy levels with respect to the conduction band (CB) and the valence band (VB) of the host compound.

Great progress has been made to locate the electronic states of divalent and trivalent lanthanide ions within the band gap of inorganic compounds. Thiel *et al*. studied the $4f^n$ ground state (GS) binding energies of trivalent lanthanides in garnets using resonant photoemission spectroscopy.[1–3] The energy difference between the GS of lanthanides and the bottom of the CB in other compounds was determined by photoconductivity and excited state absorption measurements.[4,5] The photon energy required to transfer an electron from the VB to a trivalent lanthanide ion is another simple but useful approach to determine the GS positions of the created divalent lanthanide relative to the top of the VB.[6–8] Once the position of the levels for only one lanthanide ion is known, the position of $4f$ and $5d$ levels of all other 13 lanthanides can be determined fairly well by using an empirical model developed by Dorenbos.[6–10]

Besides quantum efficiency, the position of the ground and excited states of lanthanides relative to the CB and VB determine whether a lanthanide impurity can act as an electron trap, electron donor, hole trap, or hole donor. Thermoluminescence (TL) has been widely used to investigate the characteristics of traps in luminescent materials. The temperature of the peak maximum of a TL glow peak provides information on the depth of the charge carrier trap.[11] It is also possible to activate an inorganic compound with two different lanthanide ions, which can work together as donor-acceptor pairs.[12–15] One lanthanide then acts as a donor ($D$) that upon photon stimulation donates an electron to the conduction band, and the other acts as an acceptor ($A$).

Lanthanide activated $Y_3Al_5O_{12}$ (YAG) is one of the most important optical materials, with a wide range of applications in lasers, lighting, displays, and scintillators, due to its outstanding chemical stability, low thermal expansion and conductivity, low acoustic losses, and excellent optical properties. It is of much interest to determine the energy level location of all the lanthanides in YAG. YAG has only one type of yttrium lattice site that can be occupied by any of the trivalent lanthanide ions without the need for a charge compensator. These properties make lanthanide-doped YAG a good material to study by means of TL techniques. In Ref. 16, we have already reported on the TL properties of YAG: $Ce^{3+}$, $Yb^{3+}$, and determined the level location of $Ce^{3+}$ and $Yb^{3+}$. It was found that $Ce^{3+}$ acts as a hole trap or electron donor and $Yb^{3+}$ as an electron trap or electron acceptor. In this paper, we extend our research by selecting five other donor-acceptor pairs. In addition to $Ce^{3+}$, also $Pr^{3+}$ and $Tb^{3+}$ were selected as electron donors that were combined with $Yb^{3+}$ or $Eu^{3+}$ as electron acceptors. The aim is to construct a reliable energy level scheme for YAG containing the ground and excited states of all 14 divalent and all 14 trivalent lanthanide ions.

## II. EXPERIMENTAL

### A. Sample preparation

Powder samples of $(Y_{0.997}RE_{0.003})_3Al_5O_{12}$ (RE = $Ce^{3+}$, $Pr^{3+}$, and $Tb^{3+}$) and $(Y_{0.998}D_{0.001}A_{0.001})_3Al_5O_{12}$ (D = $Ce^{3+}$, $Pr^{3+}$, and $Tb^{3+}$, A = $Yb^{3+}$ and $Eu^{3+}$) were prepared by the coprecipitation technique.[17] Rare earth oxides ($Y_2O_3$, $CeO_2$, $Pr_6O_{11}$, $Tb_4O_7$, $Yb_2O_3$, and $Eu_2O_3$) of 99.999% purity and $Al(NO_3)_3$ were used as starting materials. Rare earth nitrate [$RE(NO_3)_3$] solutions (0.2 mol/l) were obtained by dissolving the corresponding rare earth oxides in 3.0 mol/l $HNO_3$ solutions. The stoichiometric mixtures of the [$RE(NO_3)_3$] solutions (0.2 mol/l) and $Al(NO_3)_3$ solution (1.0 mol/l) were mixed. The diluted $NH_3{\cdot}H_2O$ solution (5.0 mol/l) was added dropwise to adjust the pH value ≈9 during vigorous stirring. The resulting precipitate was centrifuged and washed with distilled water and ethanol and then dried at 80 °C. The precursors were calcined using a muffle furnace in CO atmosphere for 2 h at 1250 °C. X-ray powder diffraction of the samples were made, and impurity phases were not detected.

 

### B. Measurement techniques

The TL measurements were performed with a Risø TL/OSL reader model TL/OSL-DA-15A/B with an EMI 9635QA PM tube with a BG39 filter in front of it. The filter transmits in the 330- to 600-nm region, which covers the possible $Ce^{3+}$ $5d$-$4f$ emission near 540 nm, the possible $Tb^{3+}$ $4f$-$4f$ emission at 545 nm, the possible $5d$-$4f$ emission of $Pr^{3+}$ between 300 and 400 nm, and the possible $4f$-$4f$ emission of $Pr^{3+}$. The black body radiation in infrared is blocked by the filter. Irradiations were performed with $\beta$ particles from a $^{90}Sr/^{90}Y$ source installed at the reader. The $\beta$ source produces a dose rate of 1.0 mGy $s^{-1}$ at the sample position. The heating rates varied from 0.04 to 5.0 °C/s. All TL measurements were performed in a nitrogen atmosphere.

The TL emission spectra vs temperature, i.e. the so-called $\lambda T$-contour plots, were measured after the samples were exposed to 2.5 kGy from an external $^{60}Co$ source. The emitted light of each sample was detected by an UV-VIS spectrometer (Ocean Optics, QE65000) with an HR composite grating (300 lines/mm) and an entrance aperture of 100 $\mu$m, resulting in a 3.3-nm [full width at half maximum (FWHM)] wavelength resolution in the 200–800-nm spectral range. During operation, the CCD detector of the spectrometer (Hamamatsu S7031-1006, back-thinned FFT-CCD) was cooled 40 °C below ambient temperature. The spectrometer was equipped to the Risø reader, and the combined system was operated under Labview control, allowing measurement of emission spectra during heating.

A recently constructed fully automated TL-excitation facility has been described in detail in Ref. 18. In these experiments, the sample was first illuminated during 240 s with a monochromatic photon beam produced with a 150W Xenon arc lamp (Hamamatsu L2273) filtered by a 1/8-m monochromator (Oriel Cornerstone 130) with wavelength resolution of 0.8-nm/0.1-mm slit width. The beam was coupled to the Risø reader with a UV-quartz optical fiber bundle (LLB592). During the illumination phase, traps were filled with charge carriers, and afterwards, the TL was recorded with a 2-in 9235QB photomultiplier tube possessing a bialkali-type photocathode sensitive in the 200–650-nm wavelength region. The monochromatic wavelength was varied, and each time, a TL readout was performed. The integral intensity of a specific TL glow peak as a function of illumination wavelength then provides the thermoluminescence excitation spectroscopy (TLES), revealing what photon energies are required to fill the traps. The presented TLES has been corrected by the intensity of the illumination beam at the exit of the optical fiber bundle, which was calibrated with an optical power meter system (Thorlabs S120 UV silicon sensor coupled to a PM100 console).

## III. RESULTS

Figure 1 shows the TL glow curves of nine different lanthanide-doped YAG samples. The TL glow peaks can be classified by the temperature $T_m$ of the maximum in the peaks. The three single-doped samples, YAG: $Ce^{3+}$, YAG: $Pr^{3+}$, and YAG: $Tb^{3+}$ in Figs. 1(a)–1(c) display a main glow at $T_m$ = 140 °C. The three double-doped samples with fixed $A$ = $Yb^{3+}$ in Figs. 1(d)–1(f) each show a glow peak at $T_m$ near 195 °C. The three double-doped samples with fixed $A = Eu^{3+}$ in Figs. 1(g)–1(i) present glow peak positions varying from 300 to 330 °C.

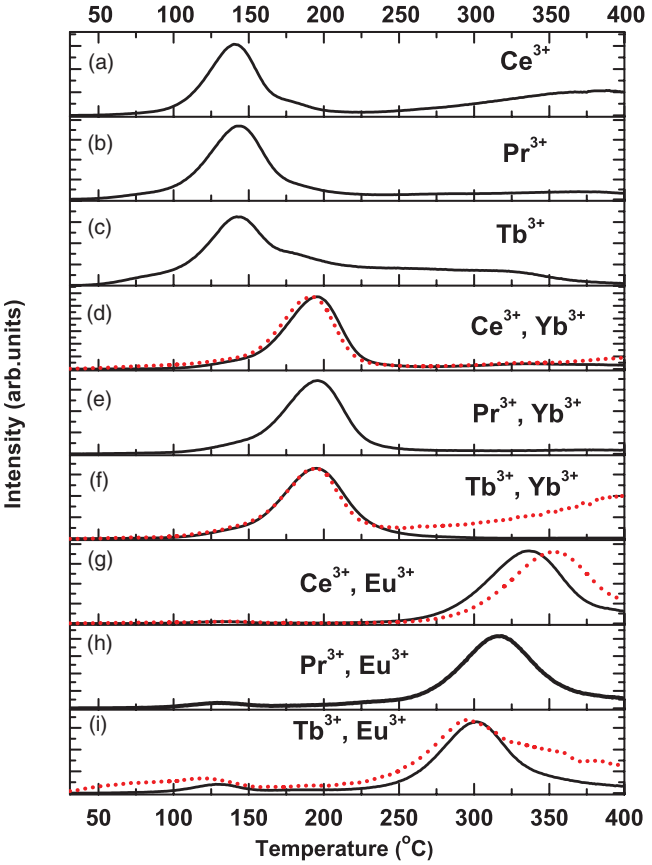


FIG. 1. (Color online) Normalized TL glow curves of (a) YAG: $Ce^{3+}$, (b) YAG: $Pr^{3+}$, (c) YAG: $Tb^{3+}$, (d) YAG: $Ce^{3+}$, $Yb^{3+}$, (e) YAG: $Pr^{3+}$, $Yb^{3+}$, (f) YAG: $Tb^{3+}$, $Yb^{3+}$, (g) YAG: $Ce^{3+}$, $Eu^{3+}$, (h) YAG: $Pr^{3+}$, $Eu^{3+}$, and (i) YAG: $Tb^{3+}$, $Eu^{3+}$ after 600-mGy $\beta$ irradiation (solid line) and after excitation with photons (red/dark gray dotted lines) with the following wavelengths: in (d) and (g), $\lambda$ = 340 nm, and in (f) and (i), $\lambda$ = 228 nm. The samples with $Pr^{3+}$ do not show a glow peak after excitation with $\lambda$ = 240 nm. The heating rate $\beta$ = 2 °C/s.

The dotted TL glow curves for the $Ce^{3+}$-$Yb^{3+}$ and $Ce^{3+}$-$Eu^{3+}$ pairs obtained upon excitation with 340-nm photons coincide with those obtained with $\beta$ irradiation. The same applies for the $Tb^{3+}$-$Yb^{3+}$ and $Tb^{3+}$-$Eu^{3+}$ pairs after excitation with 228-nm photons. It is interesting to note that, for $Pr^{3+}$-$Yb^{3+}$, no TL glow peak at 195 °C is observed upon excitation at 240 nm. We would like to add that the 140 °C glow peak observed for the three single-doped compounds is much less intense than the TL for the double-doped compounds.

Figure 2 displays the wavelength-resolved TL of the samples in a two-dimensional $\lambda T$-contour plot. For the single-doped samples in Figs. 2(a)–2(c), the TL originates from the emission of the single-dopant lanthanide ion. The glow of YAG: $Ce^{3+}$ originates from the characteristic $5d \rightarrow 4f$ emission of $Ce^{3+}$ centered at 540 nm. The main TL of YAG: $Pr^{3+}$ is near 612 nm and is attributed to the $^1D_2 \rightarrow {}^3H_4$ transition in $Pr^{3+}$. The $5d$-$4f$ emission expected between 300 and

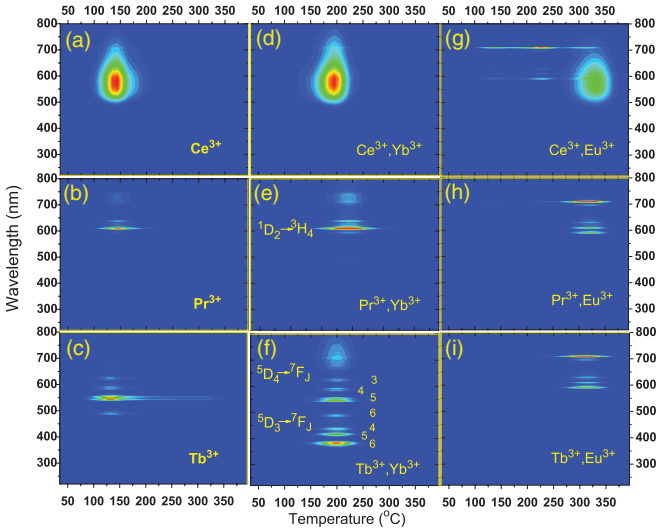


FIG. 2. (Color online) $\lambda T$-contour plots of (a) YAG: $Ce^{3+}$, (b) YAG: $Pr^{3+}$, (c) YAG: $Tb^{3+}$, (d) YAG: $Ce^{3+}$, $Yb^{3+}$, (e) YAG: $Pr^{3+}$, $Yb^{3+}$, (f) YAG: $Tb^{3+}$, $Yb^{3+}$, (g) YAG: $Ce^{3+}$, $Eu^{3+}$, (h) YAG: $Pr^{3+}$, $Eu^{3+}$, and (i) YAG: $Tb^{3+}$, $Eu^{3+}$ after exposure to irradiation of 2.5 kGy from a $^{60}$Co source. The heating rate is $\beta = 2$ °C/s.

400 nm and emission from the $^3P_0$ level is not visible in the $\lambda T$-contour plot. The TL of YAG: $Tb^{3+}$ is due to the characteristic $^5D_4 \rightarrow {}^7F_J$ and $^5D_3 \rightarrow {}^7F_J$ ($J = 3, \ldots, 6$) transitions of $Tb^{3+}$. The most intense emission at 545 nm is due to the $^5D_4 \rightarrow {}^7F_5$ transition.

Adding $Yb^{3+}$ as an extra impurity, the TL emissions in Figs. 2(d)–2(f) are at the same wavelengths as for the corresponding single-doped samples, but the glow peaks are located at higher temperatures than in Fig. 1. For the $Tb^{3+}$-$Yb^{3+}$ pair, one observes that the strongest emission is from the $^5D_3 \rightarrow {}^7F_6$ transition and not from the $^5D_4 \rightarrow {}^7F_5$ transition observed for the single Tb-doped sample. Considering the low $Tb^{3+}$ concentration in our samples (YAG: 0.3% $Tb^{3+}$ and YAG: 0.1% $Tb^{3+}$, 0.1% $Yb^{3+}$), the $Tb^{3+}$ emission in YAG dominantly from the $^5D_3$ level is to be expected.[19] Why it is quenched in the TL glow of the YAG: 0.3% $Tb^{3+}$ sample is not clear yet.

Replacing $Yb^{3+}$ for $Eu^{3+}$ gives the contour plots shown in Figs. 2(g)–2(i). The contour plot for the $Ce^{3+}$-$Eu^{3+}$ pair in Fig. 2(g) contains the $Ce^{3+}$ $5d \rightarrow 4f$ emission near 340 °C but also $Eu^{3+}$ $^5D_0 \rightarrow {}^7F_J$ emissions near 225 °C. The $Eu^{3+}$ emission spectra are dominated by the $^5D_0 \rightarrow {}^7F_4$ transition at 710 nm, which is typical for garnet compounds due to the point symmetry at the yttrium site.[20] In Fig. 1(g), that also pertains to the $Ce^{3+}$- and $Eu^{3+}$-doped sample; the 340 °C glow peak is present, but that at 225 °C is absent. That is because the TL reader in the experiment of Fig. 1 is insensitive to the main $Eu^{3+}$ emission at 710 nm and due to the used filter (BG39).

Figure 3 shows a cross section of the results in Figs. 2(g)–2(i) made at a temperature of 335 °C. The intensity of the $Ce^{3+}$ $5d \rightarrow 4f$ emission is much stronger than that of the fairly weak $Eu^{3+}$ emission lines. Most likely, the weak $Eu^{3+}$ is connected with the 225 °C trap and not the 335 °C trap. Figures 3(b) and 3(c) show that, for the other two samples, the main emission is from $Eu^{3+}$ between 580 and 720 nm. $Pr^{3+}$ and

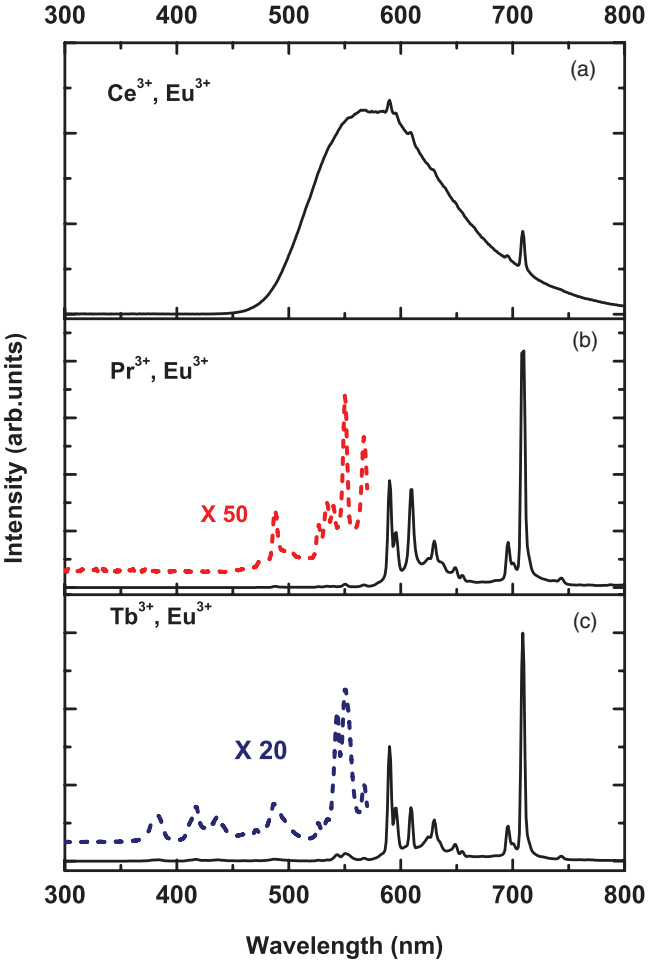


FIG. 3. (Color online) TL emission spectra of (a) YAG: $Ce^{3+}$, $Eu^{3+}$, (b) YAG: $Pr^{3+}$, $Eu^{3+}$ (the dotted line is shown with a factor of 50 enlarged intensity), and (c) YAG: $Tb^{3+}$, $Eu^{3+}$ (the dotted line is shown with a factor of 20 enlarged intensity) at 335 °C.

$Tb^{3+}$ emission is present; however, it is about a factor of 50 to 20 times weaker than the emission from $Eu^{3+}$.

The activation energy associated with the main TL glow peaks was determined with the variable heating rate method employing the relation:[21]

$$\beta E / k_B T_m^2 = s \exp(-E/k_B T_m). \quad (1)$$

Here $\beta$ (K/s) is the heating rate, $E$ (eV) is the activation energy or trap depth, $k_B$ is the Boltzmann constant, $T_m$ (K) is the temperature at which the glow curve has maximum intensity, $s$ ($s^{-1}$) is the frequency factor. Plotting $\ln(T^2{}_m/\beta)$ against $1/k_B T_m$ should result in a straight line with slope $E$. Figure 4 presents the heating rate plots, and indeed it shows straight lines. For YAG: $Pr^{3+}$, $Yb^{3+}$, and YAG: $Tb^{3+}$, $Yb^{3+}$, the two lines overlap perfectly, and that of YAG: $Ce^{3+}$, $Yb^{3+}$ runs closely parallel. The three lines for A = $Eu^{3+}$ are also parallel to each other, indicating that activation energies $E$ are similar but with different frequency factors. The values of $E$ and the frequency factor $s$ as derived from the heating rate plots are compiled in Table I. The activation energy for the TL glow in the three samples with $A = Yb^{3+}$ is 1.20 eV. The glow is attributed to the release of electrons from $Yb^{2+}$ that recombine with $Ce^{4+}$. It is concluded that the $Yb^{2+}$ ground

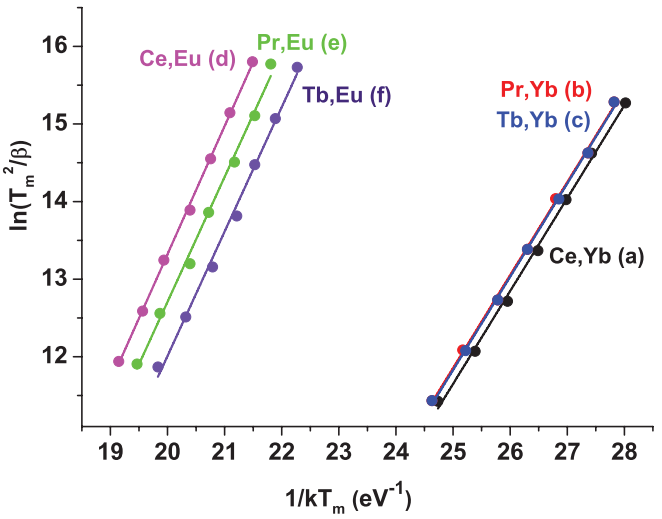


FIG. 4. (Color online) Heating rate plots of (a) YAG: $Ce^{3+}$, $Yb^{3+}$, (b) YAG: $Pr^{3+}$, $Yb^{3+}$, (c) YAG: $Tb^{3+}$, $Yb^{3+}$, (d) YAG: $Ce^{3+}$, $Eu^{3+}$, (e) YAG: $Pr^{3+}$, $Eu^{3+}$, and (f) YAG: $Tb^{3+}$, $Eu^{3+}$ after $\beta$ irradiation.

state is about 1.2 eV below the bottom of the conduction band. Similarly, the ground state of $Eu^{2+}$ must be 0.40 to 0.45 eV lower than the ground state of $Yb^{2+}$.

Figure 5 shows the TL excitation spectra (TLES) of $Yb^{2+}$ creation in YAG: $Ln^{3+}$ $Yb^{3+}$ ($Ln^{3+}$ = $Ce^{3+}$, $Pr^{3+}$, and $Tb^{3+}$). One distinct band centered at 228 nm is observed for YAG: $Tb^{3+}$, $Yb^{3+}$ in Fig. 5(a). Three bands peaked at 342, 258, and 232 nm are observed in the TLES for YAG: $Ce^{3+}$, $Yb^{3+}$ in Fig. 5(b). No bands were observed for YAG: $Pr^{3+}$, $Yb^{3+}$ in Fig. 5(c), nor when the excitation was performed with the sample at 125 °C.

## IV. DISCUSSION

### A. Thermoluminescence properties

The single-doped samples in Figs. 1(a)–1(c) each show a main glow at $T_m$ = 140 °C. $Ce^{3+}$, $Pr^{3+}$, and $Tb^{3+}$ are known to be efficient hole traps, and since the TL emission, see Figs. 2(a)–2(c), originates from $Ce^{3+}$, $Pr^{3+}$, and $Tb^{3+}$, it is concluded that an electron is released from a trap that is not related to the dopant. We therefore attribute the 140 °C TL glow peak to a host-related electron trap. This also explains why the same TL glow is weakly present in Figs. 1(d)–1(i).

TABLE I. The activation energy $E$ (eV) as derived from the heating rate plot and the frequency factor $s$ ($s^{-1}$) as calculated from the $E$, $T_m$, and $\beta$.

| Sample | $T_m$ (K) ($\beta$ = 2 K/s) | $E$ (eV) | $s$ ($10^{12}s^{-1}$) |
|---|---|---|---|
| YAG:$Ce^{3+}$,$Yb^{3+}$ | 468 | 1.20 ± 0.03 | 1.2 ± 0.2 |
| YAG:$Pr^{3+}$,$Yb^{3+}$ | 469 | 1.20 ± 0.02 | 1.0 ± 0.5 |
| YAG:$Tb^{3+}$,$Yb^{3+}$ | 468 | 1.20 ± 0.02 | 1.1 ± 0.6 |
| YAG:$Ce^{3+}$,$Eu^{3+}$ | 609 | 1.65 ± 0.02 | 4.7 ± 2.0 |
| YAG:$Pr^{3+}$,$Eu^{3+}$ | 589 | 1.61 ± 0.05 | 6.4 ± 4.0 |
| YAG:$Tb^{3+}$,$Eu^{3+}$ | 574 | 1.60 ± 0.05 | 12.6 ± 4.0 |

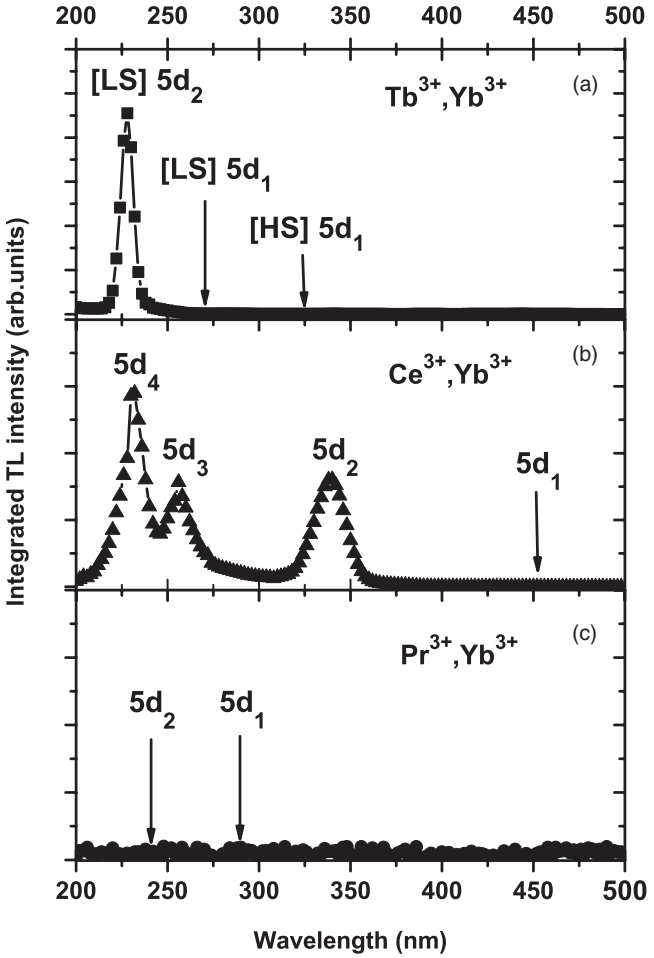


FIG. 5. TL excitation spectra of (a) YAG: $Tb^{3+}$, $Yb^{3+}$, (b) YAG: $Ce^{3+}$, $Yb^{3+}$, and (c) YAG: $Pr^{3+}$, $Yb^{3+}$ at room temperature. The arrows indicate the positions of the absent 5*d* bands.

The TL glow peak at 195 °C for the three samples with $A$ = $Yb^{3+}$ is attributed to the release of electrons trapped at $Yb^{2+}$, which then generates the observed $Ce^{3+}$, $Pr^{3+}$, and $Tb^{3+}$ emissions in Figs. 2(d)–2(f). Something similar applies to the three samples with $A$ = $Eu^{3+}$, where the glow peaks in Figs. 1(g)–1(i) with $T_m$ ranging from 300 to 340 °C are attributed to the release of electrons trapped at $Eu^{2+}$. Like in the case of $A$ = $Yb^{3+}$, one expects emission from $Ce^{3+}$, $Pr^{3+}$, and $Tb^{3+}$; this is indeed observed in Fig. 3. For $Ce^{3+}$, there is no significant emission from $Eu^{3+}$, but for Pr and Tb, there is also emission from $Eu^{3+}$ that appears at a factor of 50 to 20 times stronger. It suggests that, although electrons are supposed to be released from $Eu^{2+}$ to recombine with holes trapped at or near $Pr^{3+}$ or $Tb^{3+}$, somehow the recombination energy is efficiently transferred to a nearby $Eu^{3+}$ center. This will be discussed further below.

### B. Location of the $Ln^{2+}$ ground state levels

From the results in Table I, we concluded that the $Yb^{2+}$ ground state is located about 1.20 eV and that of $Eu^{2+}$ about 1.62 eV below the bottom of the conduction band (CB). The ground state location can also be derived from the energy of electron transfer $E^{CT}$ from the valence band to $Ln^{3+}$. There are several reports on the CT energies into $Eu^{3+}$ and $Yb^{3+}$ in YAG.

The value for $Yb^{3+}$ is $(5.9 \pm 0.1)$ eV [22–24] and for $Eu^{3+}$ $(5.5 \pm 0.2)$ eV.[22,25–27] The band gap $E_{VC}$, i.e. the energy difference between the bottom of the CB or mobility edge and the top of the valence band, can be estimated from the energy of the host exciton creation, which is about 6.95 eV.[28,29] To reach the mobility edge the binding energy of the exciton still needs to be added, which is estimated about 8% of the exciton energy resulting in $E_{VC} = 7.5$ eV. The two CT energies therefore suggest that the GS of $Yb^{2+}$ and $Eu^{2+}$ are 0.4 eV deeper below the CB than as suggested by the TL activation energies. Such a difference can be due to systematic errors in both the TL and the CT method. The mobility edge pertains to undoped YAG at low temperature of 10–50 K, whereas the TL-derived trapping depth pertains to a temperature higher than 450 K, typical for the heating rate method. It is known that the band gap of compounds tend to reduce by several tenths of eV as the temperature increases, and also the lanthanide impurities may affect the bottom of the CB.

When the energy difference between the GS of $Eu^{2+}$ and the top of the VB is known, the location of the GSs of all other divalent lanthanide ions can be obtained by using the relation:[6]

$$E_{Vf}(n+1,2+,A) = E^{CT}(6,3+,A) + \Delta E^{CT}(n,6,3+). \tag{2}$$

Here, $n$ is the number of electrons in the $4f$ shell of $Ln^{3+}$, $E_{Vf}$ $(n+1, 2+, A)$ is the energy difference between the top of the VB of host compound $A$ and the $4f^{n+1}$ GS of the divalent lanthanide ion, $\Delta E^{CT}(n, 6, 3+)$ is the average energy difference between the CT to $Ln^{3+}[4f^n]$ and to $Eu^{3+}[4f^6]$ as observed in compounds. The most recent values for all lanthanides compiled in Ref. 30 were used. The value of $\Delta E^{CT}$ (13, 6, 3+) for $Yb^{3+}$ is 0.44 eV, which implies that $Yb^{3+}$ traps electrons 0.44 eV less deeply than $Eu^{3+}$ does.[6] This agrees nicely with the difference of 0.4 eV in the activation energies found for the release of electrons from $Eu^{2+}$ and $Yb^{2+}$ in this paper.

The $4f^{n+1}$ GSs of all the divalent lanthanide ions in YAG as determined by Eq. (2) are shown in Fig. 6. The top of the VB is chosen as zero energy, and the mobility edge of YAG is placed at 7.5 eV. The double zigzag curve that connects the GS energy levels of the divalent lanthanides is pinned by the observed energies of CT to $Eu^{3+}$ and $Yb^{3+}$ as further indicated by arrow (1) and (2) with ends at 5.5 and 5.9 eV.

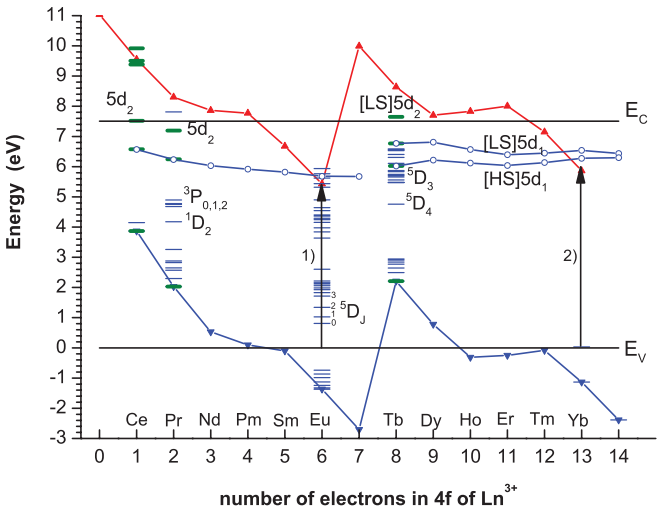


FIG. 6. (Color online) Energy level scheme of the lanthanides in YAG.

### C. Location of the $Ln^{3+}$ ground state levels

To locate the GS levels of the trivalent lanthanides, use will be made of the results from the TLES shown in Fig. 5. For YAG: $Tb^{3+}$, $Yb^{3+}$, Fig. 5(a), one band centered at 228 nm is observed. This band is attributed to the second dipole and spin allowed $4f^8 \rightarrow 4f^7 5d$ excitation in $Tb^{3+}$ that is known to be located at 228 nm.[31] The transition ends at the so-called low-spin [LS]$5d_2$ state, which energy must be either inside or close below the CB, enabling escape of the electron into the conduction band at room temperature and subsequent trapping by $Yb^{3+}$. The first spin allowed $Tb^{3+}$ $4f^8 \rightarrow 4f^7 5d$ transition to the [LS]$5d_1$ state is at 272 nm and the first spin forbidden $4f^8 \rightarrow 4f^7 5d$ transition to the high-spin [HS]$5d_1$ state at 325 nm.[31] In the TLES, these two bands are not observed. It evidences that the [HS]$5d_1$ and [LS]$5d_1$ levels are located sufficiently far below the CB to prevent thermal ionization at room temperature.

For YAG: $Ce^{3+}$, $Yb^{3+}$, Fig. 5(b) reveals three strong TLES bands at 342, 258, and 232 nm, which must be attributed to the excitation from the $4f^1$ ground state of $Ce^{3+}$ to the $5d_2$, $5d_3$, and $5d_4$ excited states.[32] The $5d_1$ excitation of $Ce^{3+}$ occurs at 457 nm, but it is not present as a band in the TLES. We conclude that the $5d_3$ and $5d_4$ levels are definitely inside the CB, and the $5d_2$ level is either within or very close below the bottom of the CB. The lowest $5d_1$ state must be well below the CB. It is interesting to compare our result with the photocurrent excitation spectrum of YAG: $Ce^{3+}$.[33] In the photocurrent spectrum, both $5d_1$ and $5d_2$ bands are absent, while in our TLES spectrum, only the $5d_1$ band is absent. The difference must be due to the presence of $Yb^{3+}$, and apparently, the excitation energy needed to produce a photocurrent is somewhat larger than the energy needed to raise the electron into the conduction band with subsequent trapping at a $Yb^{3+}$ site. It indicates that the $5d_2$ level must be very close to the bottom of the conduction band.

The first $5d_1$ and $5d_2$ excitation bands of $Pr^{3+}$ in YAG are at 290 and 240 nm.[34] The fact that no single $Pr^{3+}$ TLES band is observed between 200 and 500 nm in Fig. 5(c) evidences that these levels must be located below the CB.

With the knowledge from the TLES spectra, it is possible to draw the energy levels of all the trivalent lanthanide ions relative to the CB and VB of YAG fairly well by using the equation:[35]

$$E_{vf}(Ln^{3+},A) = E_{vf}(Ce^{3+},A) + \Delta E_{vf}(Ln^{3+}). \tag{3}$$

Here, $E_{vf}(Ln^{3+}, A)$ is the energy of the $4f^n$ ground state of the trivalent lanthanide above the valence band, $\Delta E_{vf}(Ln^{3+})$ is a compound-independent energy difference between the GS of $Ln^{3+}$ with the GS of $Ce^{3+}$. Values as compiled in Ref. 30 were used for the lanthanides $Ce^{3+}$ to $Gd^{3+}$. For the heavy lanthanides $Tb^{3+}$ to $Lu^{3+}$, both the [HS]$5d_1$ and [LS]$5d_1$ level locations are shown in Fig. 6. The levels are pinned in the scheme by placing the $5d_2$ state of $Ce^{3+}$ at the bottom of the conduction band, which then also pins the $4f$ ground state

of $Ce^{3+}$ and that of all other trivalent lanthanides. Once the ground state levels are placed, also the excited 5*d* levels can be drawn in the scheme. Figure 6 is now fully consistent with the observations made. The 6.77-eV [LS]$5d_1$ energy of $Tb^{3+}$ is well below and the 7.65-eV [LS]$5d_2$ energy is well above $E_C$, consistent with the TLES of Fig. 5(a). The 6.25-eV $5d_1$ energy and 7.19-eV $5d_2$ energy of $Pr^{3+}$ are both well below $E_C$, explaining the absence of TLES bands in Fig. 5(c). The 7.5-eV $5d_2$ energy of $Ce^{3+}$ coincides with $E_C$, causing a band in the TLES of Fig. 5(b). However, the electron escape probability to generate a photocurrent appears not yet sufficient.[33]

What still needs to be explained is the dominance of $Eu^{3+}$ emission in the recombination luminescence of the $Pr^{3+}$, $Eu^{3+}$- and $Tb^{3+}$, $Eu^{3+}$-doped samples in Figs. 3(b) and 3(c). Knowing that the recombination takes place at $Pr^{3+}$ or $Tb^{3+}$, there is apparently an efficient energy transfer to $Eu^{3+}$. One may think of a Forster–Dexter type of transfer from the $^3P_0$ level of $Pr^{3+}$ and the $^5D_3$ or $^5D_4$ levels of $Tb^{3+}$. The scheme suggests a second possible explanation for the very weak $Pr^{3+}$ and $Tb^{3+}$ and strong $Eu^{3+}$ TL emission intensity. The $Pr^{3+}$ and $Tb^{3+}$ ground states are 5.5 and 5.3 eV below the conduction band, which implies that the same amount of energy is available during the electron hole recombination. This energy is resonant with the energy of 5.45 eV for CT to $Eu^{3+}$, which then may induce a very efficient energy transfer, also of the Forster–Dexter type, to a nearby $Eu^{3+}$ center. This transfer route may be more effective because the CT band of $Eu^{3+}$ is dipole allowed, whereas that of the $4f$-$4f$ transition in $Eu^{3+}$ are dipole forbidden. In the case of $Ce^{3+}$, 1.6 eV less recombination energy is available, and transfer via the CT band of $Eu^{3+}$ is not possible. Furthermore, the lifetime of the $Ce^{3+}$ 5*d* state is orders of magnitude shorter than that of the $Pr^{3+}$ and $Tb^{3+}$ excited states, which makes energy transfer less probable. This all is consistent with the absence of strong $Eu^{3+}$ emission in Fig. 3(a). For $Yb^{3+}$ with the CT band at 5.9 eV and absence of $4f^{13}$ excited states, energy transfer to $Yb^{3+}$ by means of the CT band or high-energy $4f^{13}$ levels is not likely, and the TL glow will be from $Pr^{3+}$ and $Tb^{3+}$.

## V. CONCLUSIONS

In this paper, the thermoluminescence properties of YAG doped with lanthanide electron donor and acceptor pairs have been studied. $Eu^{3+}$ and $Yb^{3+}$ trap electrons from the CB, while $Ce^{3+}$, $Pr^{3+}$, and $Tb^{3+}$ act as hole traps or electron donors. During a TL readout, the trapped electrons are thermally activated from $Eu^{2+}$ and $Yb^{2+}$ to recombine via the CB with $Ce^{4+}$, $Pr^{4+}$, and $Tb^{4+}$. As a result, the characteristic emission of $Ce^{3+}$, $Pr^{3+}$, and $Tb^{3+}$ are observed. The activation energies for electron release from $Eu^{2+}$ and $Yb^{2+}$ derived from TL glow peaks are in satisfactory agreement with the values estimated from the $O^{2-} \rightarrow Eu^{3+}$ and $O^{2-} \rightarrow Yb^{3+}$ CT energy. The thermal luminescence excitation technique has been applied to derive information on the location of $4f^n$ ground states of $Ce^{3+}$, $Pr^{3+}$, and $Tb^{3+}$. The information from the TL and the TLE spectra has been used as input for a model to construct a scheme with the location of the energy levels of all divalent and trivalent lanthanides in YAG. The scheme is fully consistent with the observations made.

## ACKNOWLEDGMENTS

F. You thanks the China Scholarship Council, Ministry of Education. This work is partly supported by the National Natural Science Foundation of China (Grant Nos. 10979009 and 10774012).

*Corresponding author: Dr. Fangtian You, Institute of Optoelectronic Technology, Beijing Jiaotong University, Beijing 100044, China; ftyou@bjtu.edu.cn

[1] C. W. Thiel, H. Cruguel, H. Wu, Y. Sun, G. J. Lapeyre, R. L. Cone, R. W. Equall, and R. M. Macfarlane, Phys. Rev. B **64**, 085107 (2001).
[2] C. W. Thiel, H. Cruguel, Y. Sun, G. J. Lapeyre, R. M. Macfarlane, R. W. Equall, and R. L. Cone, J. Lumin. **94/95**, 1 (2001).
[3] C. W. Thiel, Y. Sun, and R. L. Cone, J. Mod. Opt. **49**, 2399 (2002).
[4] C. Pedrini, F. Rogemond, and D. S. McClure, J. Appl. Phys. **59**, 1196 (1986).
[5] J. K. Lawson and S. A. Payne, J. Opt. Soc. Am. B **8**, 1404 (1991).
[6] P. Dorenbos, J. Phys. Condens. Matter **15**, 8417 (2003).
[7] P. Dorenbos, J. Lumin. **111**, 89 (2005).
[8] P. Dorenbos, J. Alloys Compd. **488**, 568 (2009).
[9] P. Dorenbos, J. Lumin. **108**, 301 (2004).
[10] P. Dorenbos, J. Phys. Condens. Matter **15**, 575 (2003).
[11] P. Dorenbos and A. J. J. Bos, Radiat. Meas. **43**, 139 (2008).
[12] P. Dorenbos, A. J. J. Bos, and N. R. J. Poolton, Phys. Rev. B **82**, 195127 (2010).
[13] A. H. Krumpel, A. J. J. Bos, A. Bessière, E. van der Kolk, and P. Dorenbos, Phys. Rev. B **80**, 085103 (2009).
[14] A. J. J. Bos, P. Dorenbos, A. Bessière, and B. Viana, Radiat. Meas. **43**, 222 (2008).
[15] A. H. Krumpel, E. van der Kolk, D. Zeelenberg, A. J. J. Bos, K. W. Kramer, and P. Dorenbos, J. Appl. Phys. **104**, 073505 (2008).
[16] F. T. You, A. J. J. Bos, Q. F. Shi, S. H. Huang, and P. Dorenbos, J. Phys. Condens. Matter **23**, 215502 (2011).
[17] Y. X. Pan, M. M. Wu, and Q. Su, Mater. Sci. Eng. B **106**, 251 (2004).
[18] A. J. J. Bos, R. M. van Duijvenvoorde, E. van der Kolk, W. Drozdowski, and P. Dorenbos, J. Lumin. **131**, 1465 (2011).
[19] K. Y. Jung and H. W. Lee, J. Lumin. **126**, 469 (2007).
[20] M. Bettinelli, A. Speghini, F. Piccinelli, A. N. C. Neto, and O. L. Malta, J. Lumin. **131**, 1026 (2011).
[21] A. J. J. Bos, Nucl. Instrum. Methods Phys. Res., Sect. B **184**, 3 (2001).
[22] L. van Pieterson, M. Heeroma, E. de Heer, and A. Meijerink, J. Lumin. **91**, 177 (2000).
[23] N. Guerassimova, N. Garnier, C. Dujardin, A. G. Petrosyan, and C. Pedrini, Chem. Phys. Lett. **339**, 197 (2001).
[24] I. A. Kamenskikh, N. Guerassimova, C. Dujardin, N. Garnier, G. Ledoux, C. Pedrini, M. Kirm, A. Petrosyan, and D. Spassky, Opt. Mater. **24**, 267 (2003).

[25]S. K. Ruan, J. G. Zhou, A. M. Zhong, J. F. Duan, X. B. Yang, and M. Z. Su, J. Alloys Compd. **275-277**, 72 (1998).
[26]P. Y. Jia, J. Lin, X. M. Han, and M. Yu, Thin Solid Films **483**, 122 (2005).
[27]Y. H. Wang and X. X. Li, J. Electrochem. Soc. **153**, G238 (2006).
[28]Y. Zorenko, E. Zych, and A. Voloshinovskii, Opt. Mater. **31**, 1845 (2009).
[29]V. Babin, A. Krasnikov, Y. Maksimov, K. Nejezchleb, M. Nikl, T. Savikhina, and S. Zazubovich, Opt. Mater. **30**, 30 (2007).
[30]P. Dorenbos, A. H. Krumpel, E. van der Kolk, P. Boutinaud, M. Bettinelli, and E. Cavalli, Opt. Mater. **32**, 1681 (2010).
[31]A. Mayolet, W. Zhang, E. Simoni, J. C. Krupa, and P. Martin, Opt. Mater. **4**, 757 (1995).
[32]D. S. Hamilton, S. K. Gayen, G. J. Pogatshnik, R. D. Ghen, and W. J. Miniscalco, Phys. Rev. B **39**, 8807 (1989).
[33]J. Ueda, S. Tanabe, and T. Nakanishi, J. Appl. Phys. **110**, 053102 (2011).
[34]Y. M. Cheung and S. K. Gayen, Phys. Rev. B **49**, 14827 (1994).
[35]P. Dorenbos, A. J. J. Bos, and N. R. J. Poolton, Opt. Mater. **33**, 1019 (2011).